Numerical Simulation of Internal Flashing in a GDI Injector Nozzle

Bejoy Mandumpala Devassy*[1], D. Benković[2], Z. Petranovic[1], W. Edelbauer[1], M. Vujanovic[2]
[1]AVL LIST GmbH, Graz, Austria
[2] University of Zagreb, Faculty of Mechanical Engineering and Naval Architecture, Ivana Lučića, 5, 10000 Zagreb – Croatia

*Corresponding author: Bejoy.MandumpalaDevassy@avl.com

Abstract
As global environmental issues are becoming even more critical, there is further increasing pressure on the automotive industry to develop engines with reduced emissions and better fuel economy while meeting performance requirements. One of the developments in automotive engine technology to meet these requirement is the Gasoline Direct Injection (GDI) system. Introduction of fuel at elevated temperature is a method employed which can cause the fuel to undergo flash boiling within the nozzle hole, and thereby inducing enhanced atomization. The aim of the present work is to investigate the flash boiling mechanism inside fuel injector nozzles using the advanced Hertz-Knudsen model implemented in a commercial CFD code. The model is first validated by a benchmark nozzle test case where the investigation is conducted to interpret various aspects of bubble number density and its variation with respect to the degree of superheat. The obtained results from the simulation and the one from the benchmark test case show a substantiated comparison. In the second part of this work, the flash boiling model is tested in a realistic 8-hole GDI Injector, from Engine Combustion Network database, with an attached high-pressure gas chamber. The Mass, momentum and enthalpy equations were solved for a 3-phase system (liquid fuel, fuel vapour and air) with applied interfacial exchange models between them.

Keywords
GDI Engine, Injector, Flash Boiling, Atomization.

Introduction

In a constant search for improvements in the field of internal combustion engines efficiency, with the accent on the pollutant reduction, every stage of fluid flow within the engine system needs to be known in detail. These stages account the fuel injection process, liquid – gas interaction, subsequent vapor distribution, mixing, combustion and pollutant emission production. The way the fuel is delivered in the combustion chamber is the first part of the engine operating process and has direct impact on the combustion process, which is further a direct cause of the pollutant generation. The injection process itself is the main subject of interest in this paper, where the advanced Hertz-Knudsen model [1] for describing the Flash Boiling process inside a fuel injector nozzle is implemented and investigated in AVL FIRE™ [2].

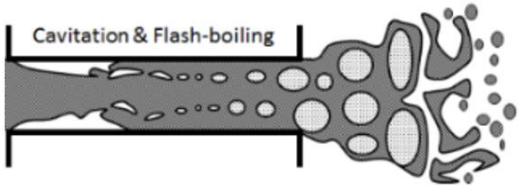

Figure 1 Schematic of general cavitation and flash boiling bubbles [3]**.**

Flash boiling is a phenomenon when the preheated liquid is depressurized to the value below the liquid saturation pressure, or in terms of temperature - a phenomenon occurring when the liquid temperature exceeds its saturation temperature [4]. The schematic of general cavitation appearing near to the nozzle inlet and flash boiling bubbles near the nozzle outlet is shown in Figure 1. Many researchers analyzed flash boiling conditions inside the combustion chamber to examine the influence of flash boiling on the mixing process. At first, the applicability of the flash boiling effect in the internal combustion engines was investigated by Gerrish and Ayer [5] by increasing the fuel temperature in a pre-chamber of a diesel engine, which resulted in a slightly increased engine efficiency. The interest for the topic was induced and until today, a deep insight of the flash boiling process is achieved. Therefore, in [6] and [7], flash boiling was analyzed for transient needle motion and for fixed needle lift positions. The results

from the numerical simulations were compared with the experimental data. Good agreement between the numerical results and experimental imaging, in terms of fuel mass fraction distribution inside the discharge volume, was achieved. Hence, performed calculations resolved the presence of uniform contact of fuel with the outer wall of counter bores. In addition, the hole-to-hole variations were examined, and a small deviation in the amount of injected fuel was noticed. A low vertical needle position has been proven to significantly affect the flow patterns in terms of local vapor distributions. According to [8], the appearance of vapor has been noticed at the narrowest passage of the computational domain, the needle seat, respectively. Moreover, transient interacting vortices were found in the injector sac filled with the fuel. Flow behavior like that results in a string flash boiling appearance, perturbations in spray angle, as well as oscillations in the mass flow rate. The latter were attributed to the presence of vapor inside the nozzle holes which was also confirmed in [9]. The impact of the injector geometry on the vapor formation at the nozzle inlet was investigated in [10], by analyzing the flash boiling operating conditions. Therefore, with the increase of the inlet radii, the formation of the cavity at the nozzle entrance is reduced. Accordingly, smaller inlet radius results in a larger flow turning angle, hence creating a cavitation region. Authors in [11] performed an experimental investigation of a five-hole gasoline direct injector spray collapse under flash boiling conditions. The Doppler measurement technique was used for examination of spray morphology and droplet dynamics. Thereby, it was determined that spray collapse occurs in the far field due to the formation of a low-pressure zone because of the temperature decrease and the resulting condensation. Furthermore, at the inner side of a target jet, i.e. closer to the injector axis, a slight increase in the droplet size was noticed. Similar investigations were carried out on six and eight-hole GDI injectors, with the emphasis on droplet size measurements [12]. The observed reduction of the mean droplet size was associated with the increase of the degree of superheat. Another experimental research of a direct fuel injection was carried out in [13],[14],[15],[16], where the spray behavior was captured by optical imaging. It was found that in order to reach the chamber pressure, fuel flow inside of the nozzle must expand rapidly, consequently vaporizing inside the counter bores. Further expansion of vaporized fuel prevents the downstream gas from entering the counter bores, and consequently, spreading of plume angle occurs. In case when the fuel expansion is significant, neighboring spray plumes are able to interfere: plume-to-plume interaction in most cases leads to spray collapse. The investigation of flash boiling regimes and spray break-up under a flash boiling condition was performed in [17],[18],[19]. The main factor which determines the efficiency of spray atomization, the degree of superheat, was therefore established. Other fluid properties, such as viscosity and surface tension, were proved to enhance the effect of spray formation and break-up.

This work is structured as follows: the next section provides the system of equations employed for the present investigation, while the advanced Hertz-Knudsen model for internal flashing is later explained in detail. Computational conditions for model validation as well as the flashing conditions in an 8-hole injector from the Engine Combustion Network (ECN) [20] is studied, and the obtained results are examined in the later sections. In the final section of this paper brief conclusions and an outlook are presented.

System of Equations

Within the theory of multi-phase flows, each phase is considered as separate continuum, where the conservation laws are applied. An ensemble averaging is used to remove the microscopic interfaces. This results in macroscopic conservation equations analogous to their single-phase counterparts. The averaged continuity, momentum and enthalpy equations, (1), (2) and (3), can be derived based on the work of Drew and Passman [21] and others:

$$\frac{\partial \alpha_k \rho_k}{\partial t} + \frac{\partial \alpha_k \rho_k V_{k,j}}{\partial x_j} = \Gamma_k \tag{1}$$

$$\frac{\partial \alpha_k \rho_k V_{k,i}}{\partial t} + \frac{\partial \alpha_k \rho_k V_{k,j} V_{k,i}}{\partial x_j} = -\alpha_k \frac{\partial P_k}{\partial x_i} + \alpha_k \rho_k g_i + \frac{\partial \alpha_k (\tau^L_{k,ij} + \tau^T_{k,ij})}{\partial x_j} + M_{k,i} + V_{int,i}\Gamma_k \tag{2}$$

$$\frac{\partial \alpha_k \rho_k h_k}{\partial t} + \frac{\partial \alpha_k \rho_k V_{k,j} h_k}{\partial x_j} = \alpha_k \frac{\partial P_k}{\partial t} + \frac{\partial \alpha_k (q^L_{k,j} + q^T_{k,j})}{\partial x_j} + h_{vis} + \alpha_k V_{k,i} \frac{\partial P_k}{\partial x_i} + H_k + h_k \Gamma_k \tag{3}$$

where α, ρ, V and P are the averaged volume fraction, density, velocity and pressure, respectively. Subscript *k* denotes the phase indicator, V_{int} is the interfacial velocity, Γ_k is the phase change rate, M_k is the interfacial momentum transfer term, and H_k is the interfacial energy transfer term. The terms $q^L_{k,j}$ and $q^T_{k,j}$ in Equation (3) are the laminar and turbulent heat flux contributions; $\frac{\lambda_k}{C_{p,k}} \nabla h_k$ and $\frac{\mu^t_k}{\sigma_T} \nabla h_k$ respectively. The superscripts *L* and *T* refer to the laminar and turbulent contributions respectively, and the subscripts *i* and *j* denotes the index of the Cartesian components. The interfacial mass exchange Γ_k in the flash boiling model is governed by the deviation from the thermodynamic-equilibrium conditions.

The term h_{vis} in Equation (3) corresponds to the work done by the irreversible viscous forces, commonly termed as viscous heating.

$$h_{vis} = \alpha_k(\tau^L_{k,ij} + \tau^T_{k,ij})\frac{\partial V_{k,i}}{\partial x_j} \tag{4}$$

$$\tau_{eff} = \mu_{eff}\left[\frac{\partial V_{k,i}}{\partial x_j} + \frac{\partial V_{k,j}}{\partial x_i}\right] - \frac{2}{3}\left(\rho_k k_k + \mu_{eff}\frac{\partial V_{k,i}}{\partial x_j}\right)I \tag{5}$$

where $\mu_{eff} = \mu^L_k + \mu^T_k$ and $\tau_{eff} = \tau^L_{k,ij} + \tau^T_{k,ij}$.

This viscous heating term is relevant in regions with high velocity gradients, which take place not only in the injector holes but also in the nozzle sac and the needle seat regions, thereby inducing friction and heating-up of the liquid.
Flash boiling model

The onset of cavitation bubbles is observed at the entrance edge of a nozzle or near the wall in regions where the flow direction is changed drastically. So the critical condition of cavitation is expressed by the pressure difference and the flow inertia. For flash boiling bubbles, the pressure falls below the saturation pressure of the liquid. This pressure depends on the temperature of the liquid, the degree of superheat ΔT_{sup} expressed by Equation (6), and becomes the primary driving force for flash boiling.

$$\Delta T_{sup} = T_l - T_{sat} \tag{6}$$

T_l is the superheated liquid temperature in the flow field, and T_{sat} is the saturation temperature at given pressure conditions. The cavitation usually starts at the nozzle inlet, but flash boiling is also observed at the nozzle outlet. When cavitation occurs inside the nozzle in a superheated liquid, cavitation bubble acts as a nucleation bubble, and flash boiling process is easily triggered.
The advanced Hertz-Knudsen model [1] is given with the following equation:

$$\dot{R} * A_b = \left(3\alpha_g\right)^{2/3}(4\pi N_b)^{1/3}\frac{(p_{sat} - p)}{\sqrt{2\pi R_g T_{int}}}. \tag{7}$$

In Equation (7), A_b is the bubble surface area, and N_b is the bubble number density. The gas constant is labelled with R_g, while p_{sat} and T_{sat} are representing the saturation pressure and the bubble interface temperature. The bubble interface temperature T_{int} is obtained from:

$$T_{int} = \frac{\alpha_l\rho_l Cp_l T_l + \alpha_g\rho_g Cp_g T_g}{\alpha_l\rho_l Cp_l + \alpha_g\rho_g Cp_g} \tag{8}$$

where indices l and g correspond to the continuous (liquid) and the dispersed (vapour) phase. The bubble number density is determined from the following equation:

$$N_b = 10^{13} * exp\left(\frac{-5.279}{\Delta T_{sup}}\right) \tag{9}$$

where the initial bubble number density is taken as 10^{13}. The number density, N_b is defined as a function of the degree of superheat
Hence, the mass interfacial exchange is given by Equation (10), where λ_{ac} represents the accommodation factor.

$$\Gamma_c = -\Gamma_d = \begin{cases} \lambda_{ac} C_e \dot{R} * A_b & (p_{sat} - p) > 0 \\ -\dfrac{\lambda_{ac}}{C_r}\dot{R} * A_b & (p_{sat} - p) < 0 \end{cases} \tag{10}$$

Computational Conditions

The validation of the implemented Hertz-Knudsen model is performed at the Edwards Pipe test case [22], also known as Edwards' pipe blowdown. This is a standard test case from the Committee for the Safety of Nuclear Installation (CSNI) [23]. It simulates the blowdown in a pipe of approximately 4m length, which contains initially hot and pressurized liquid. The water in the pipe has an initial pressure of 7.0 MPa and a temperature of 502 K which corresponds to an initial sub cooling of 56.8 K. The geometrical configuration is given in Figure 2. The transient phenomenon is initiated by the rupture of a bursting disk allowing the rapid discharge to the environment at atmospheric pressure.

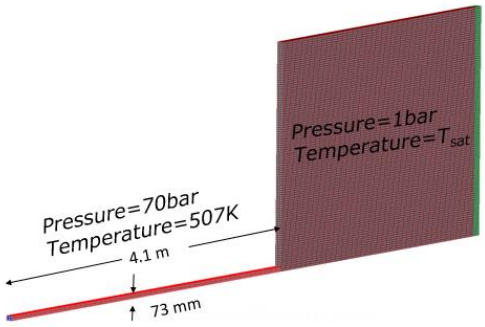

Figure 2: Edwards' pipe blowdown: computational grid and initial conditions.

Immediately after the removal of the rupture disk, a sudden pressure drop occurs at the pipe's exit resulting in the onset of violent evaporation which limits the pressure decrease to a value slightly below the saturation pressure. The governing process controlling the discharge from the pipe is the short region with extremely large evaporation rates close to the exit as created by the steep pressure gradient in this region.

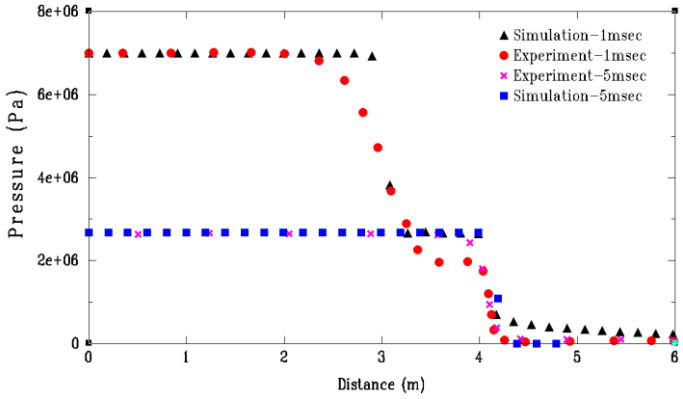

Figure 3: Edwards' pipe blowdown: parameter distributions along the pipe axis.

A comparison of the calculated values with experiments for the pressure at the pipe's head at two time instants; 1msec and 5msec, are given in Figure 3. The results show a good agreement between simulation and experiment. The second part of the investigation is carried out on a real injector geometry from ECN [20]. The computational domain, shown in Figure 4 (a), contains 1,112,576 hexahedral computational cells. The nozzle holes are O-Grid meshed, alone containing 245,760 hexahedral cells. An initial needle seat gap of 6 μm is maintained near to the needle seat occupying 8 cell layers in order to avoid cell squeezing and zero thickness cells. In Figure 4 (b) the needle lift profile employed and obtained from ECN [20] is provided. As previously stated, an interaction between the plumes was found according to [13] and [14], which is the reason for considering the complete injector geometry. As initial condition the complete injector is filled with liquid Iso-Octane preheated to 90°C at 200 bar pressure, as described in [20]. The numerical setup including the operating conditions is described in next section.

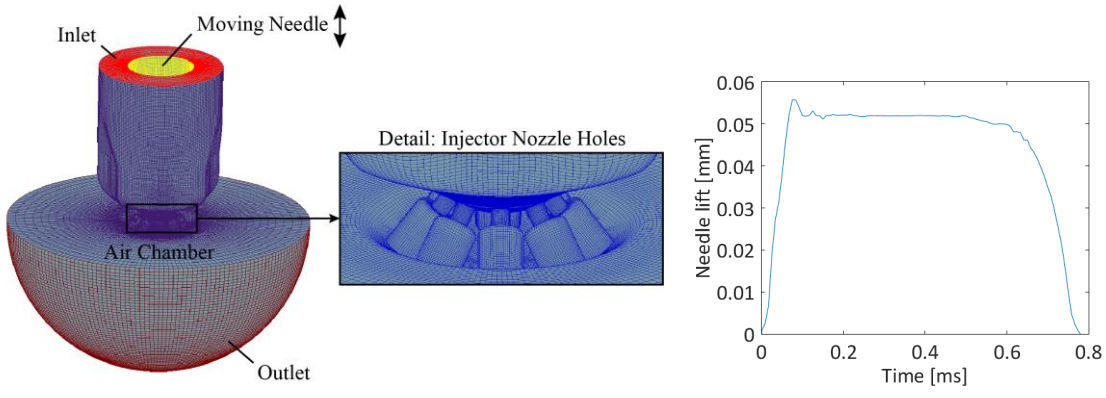

(a) (b)

Figure 4: ECN fuel injector computational domain and Needle Lift profile.

Fluid Properties, Initial and Boundary Conditions

Table 1. Fluid Properties

Properties	Liquid Phase	Vapour Phase	Gas Phase
Fluid	Iso-Octane	Iso-Octane vapour	Nitrogen
Density (kg/m^3)	690	0.5	0.5
Viscosity (Ns/m^2)	0.00214	7.5e^{-6}	1.824e^{-5}
Specific Heat Capacity (J/kgK)	2210	1375	1040
Thermal Conductivity (W/mK)	0.134	0.018	0.0257

The current analysis involves the solution of a 3 phase system: liquid Iso-Octane, Iso-Octane vapour and Nitrogen. Table 1 provides an overview about the fluid properties. The 8-hole injector is initialized with Iso-Octane liquid (α_l = 1, pressure = 200 bar), while the chamber is initialized with Nitrogen (α_g = 1, pressure = 0.5 bar and temperature = 333 K). The injector and chamber wall boundaries are considered to be adiabatic, at the chamber outer surface a pressure boundary is applied, in order to allow inflow and outflow.

Table 2. Initial Conditions

Injector	Chamber
Liquid Volume Fraction = 1	Nitrogen Volume Fraction = 1
Pressure: 200 bar	0.5 bar
Temperature: 363 K	333 K

Table 3. Boundary Conditions.

Inlet	Outlet	Wall
Pressure: 200 bar	0.5 bar	-
Temperature: 363 K	333 K	Heat Flux = 0

Table 2 and Table 3 represents the operating conditions of the simulation. The calculation is carried out for 780 micro seconds. The simulation run for 36 hrs using 20 Intel(R) Xeon(R) CPU X5620 @ 2.40GHz processors.

Results and discussion

Figure 5 shows the resulting rate of injection and mass flow rate at the nozzle hole outlet compared with experiments [20]. Figure 6 provides the time instance of Iso-Octane vapour volume fraction field from start of injection until 700 micro seconds. The high amount of vapour is generated due to the sudden de-pressurization of the system similar to the one that is obtained during the Edward's pipe [22] simulation.

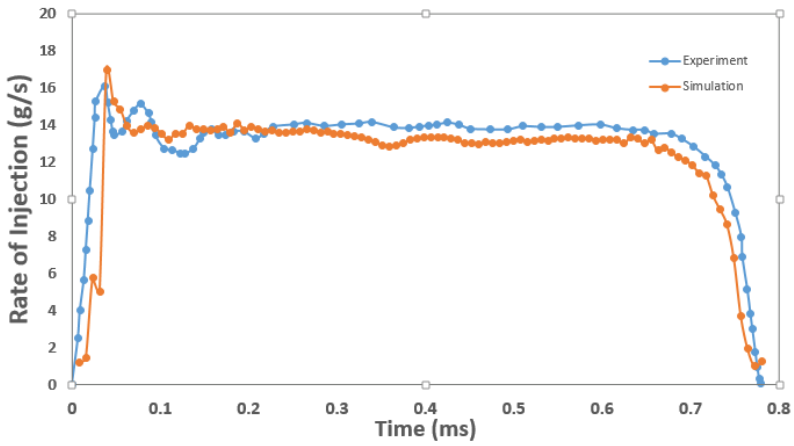

Figure 5: Rate of Injection of Spray G2 nozzle using AVL FIRE™ [2] with the Hertz Knudsen Flash Boiling model and compared with experiments [20].

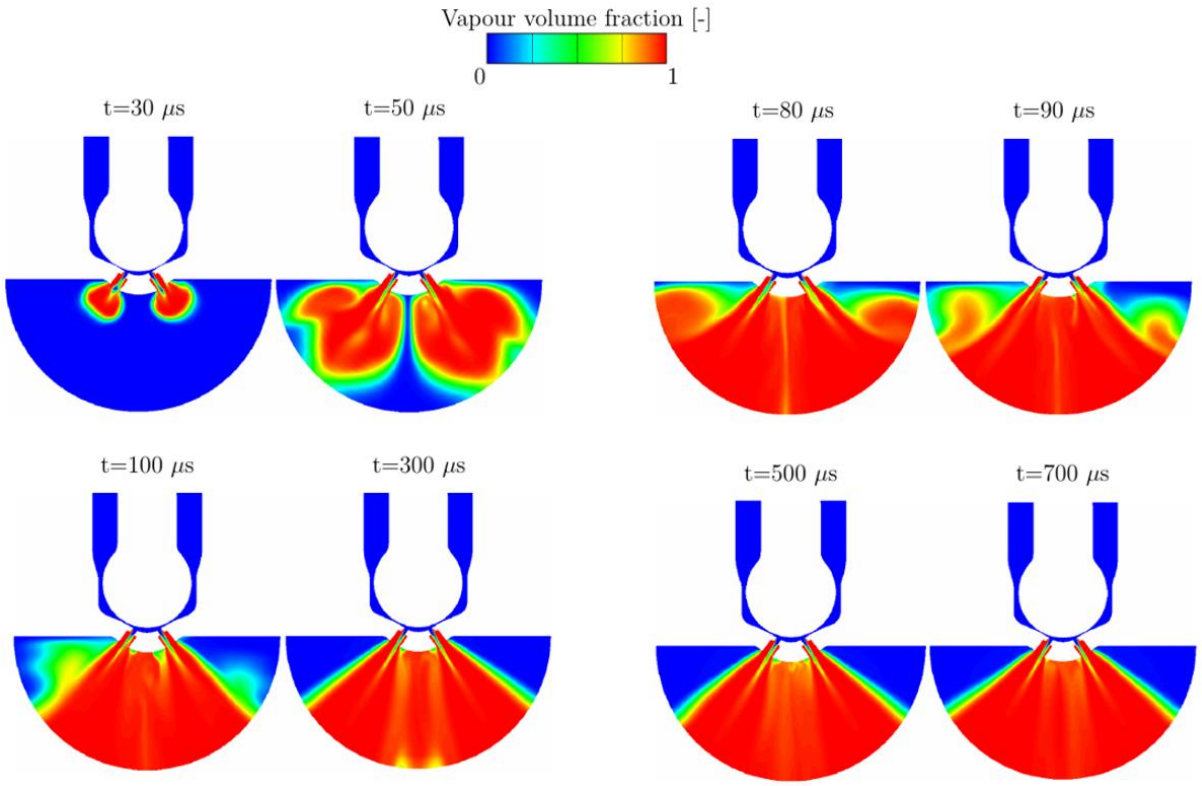

Figure 6: Time instances of Iso-Octane vapour volume fraction cloud with the Hertz-Knudsen flash boiling model from the start till the end of injection.

The vapour volume fraction distributions in Figure 6 illustrates that the vicinity of nozzles with their neighbouring nozzles has impact on the fluid flow. The influence of these neighbouring nozzles results in a large vapour plume consisting of the individual vapour clouds from each nozzle hole.

Additionally, the numerical results are compared with experimental images from of the ECN GDI spray [20]. Figure 7 shows a vapour phase obtained from the numerical simulation performed in AVL FIRE™ [2] in comparison with the spray image given in [8]. The qualitative comparison shows a good agreement between numerical simulation and experiment. In both cases, a significant plume-to-plume interaction is observed. Likewise, vapour uniformly envelops the outer counter-bores edges and the injector tip, and as a result, a thin liquid film forms on the outer side of injector once the injection process is finished. This is then later accounting for the wall wetting of nozzle tip.

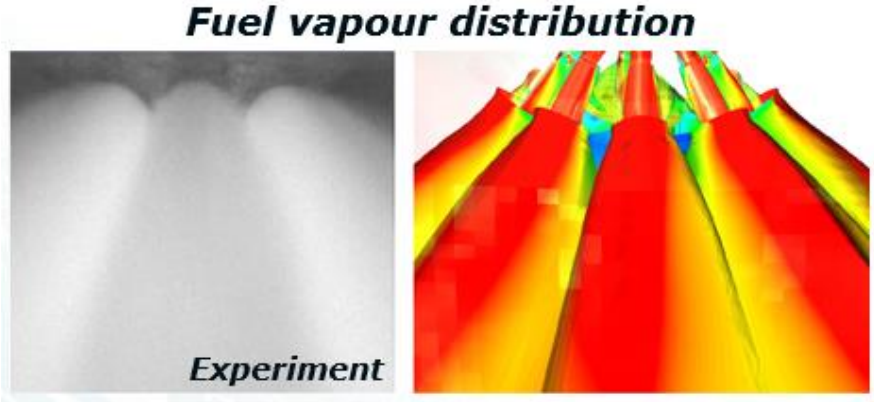

Figure 7: Iso-surface of vapour volume fraction taken in the middle of simulation (t=400 μs) and experimental imaging of ECN GDI injector [8].

Furthermore, in Figure 8 one can also observe string cavitation in the simulation which in turn influences the flow field inside the nozzle holes. These highly unsteady vapour structures, appear upstream the injector holes and inside the nozzle sac. One of the main consequences of the string cavitation is increased amount of vapour inside the nozzle, which manifests in the reduction in the individual nozzle flow rate. In Figure 8 (b), one could observe

this string vortices developed which could lead to string cavitation. Similar sightings were also observed in literature [8].

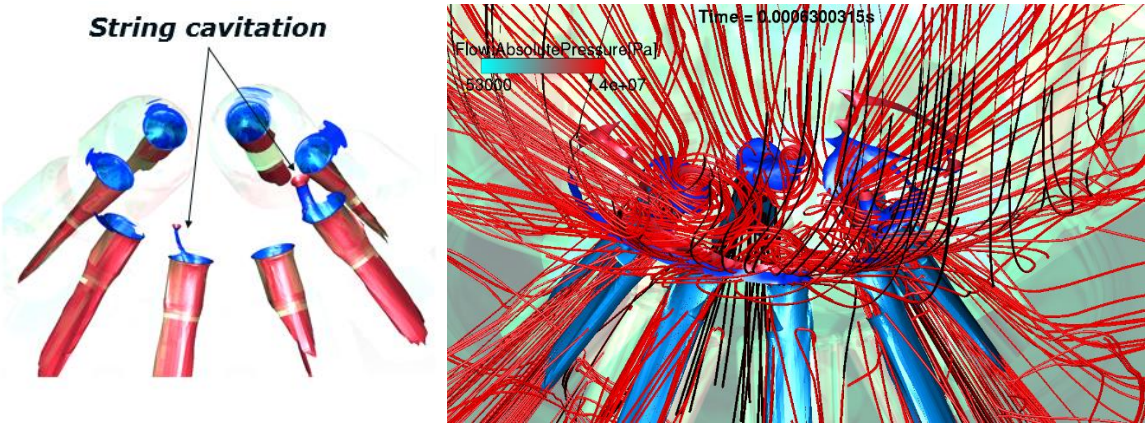

(a) (b)

Figure 8: Temporary string-cavitation appearance in the upper nozzle region.

Conclusion

This paper started by highlighting the importance of a deep understanding of the fuel injection process and the proper description of the fuel spray atomization. Accordingly, a mass exchange model, based on the Hertz-Knudsen Model [1], is proposed. This newly implemented flash boiling model in AVL FIRE™ [2], considers the mass change due to pressure differences and the degree of superheat. Initially, the model was validated using the well-known Edward's pipe blowdown test case. It was found that the flash boiling model provides a good agreement with the benchmark test case. Furthermore, the model was tested on a real 8-hole GDI injector from ECN Network [20]. In both these simulations, the flash boiling model provides blowdown and initiate the fuel for sudden vaporization due to de-pressurization. The qualitative comparison between simulation and experimental image shows good agreement. Wide spray angles as well as substantial plume-to-plume interactions were noticed. Additionally, the highly unsteady string cavitation phenomena could be detected in the simulation.

Nomenclature

P pressure [Pa]
T temperature [K]
V velocity [m s^{-1}]
h enthalpy [J kg^{-1}]
t time [s]
ρ density [kg m^{-3}]
α volume fraction
Γ mass transfer rate [kg s^{-1}]
μ viscosity [kg m^{-1} s^{-1}]
τ shear stress [Pa]

Subscripts
k general phase indicator
l liquid
ref reference values

Superscripts
L laminar
T turbulent

References

[1] Senda, J., Hojyo, Y., and Fujimoto, H., 1994, JSAE Review, 15, pp. 291-296
[2] AVL FIRE™, Eulerian Multiphase, Graz (2018).
[3] Arai, M., Senda, J., and Xu, M., Nov. 6.-9. 2016, International Conference on Liquid Atomization and Spray Systems, ILASS-Asia.
[4] Mojtabi, M., Chadwick, N., Wigley, G., and Helie, J., Sep. 8.-10. 2008, 22nd European Conference on Liquid Atomization and Spray Systems.

[5] Gerrish, B. H. C., and Ayer, B. E., 1936. Aeronautical Laboratory LM.
[6] Mohan, B., Jaasim, M., Perez, F. H., Sim, J., Roberts, W., and Im, H., May 14.-16. 2018, 10th International Symposium on Cavitation, CAV2018.
[7] Saha, K., Som, S., Battistoni, M., Li, Y., Pomraning, E., Senecal, P. K., 2016, SAE International Journal of Engines.
[8] Baldwin, E. T., Grover, R. O., Parrish, S. E., Duke, D. J., Matusik, K. E., Powell, C. F., 2016, International Journal of Multiphase Flow.
[9] Saha, K., Som, S., Battistoni, M., Li, Y., Quan, S., Senecal, P, K., 2015, Journal of Physics Conference Series.
[10] Strek, P., Duke, D., Swantek, A., Kastengren, A., Powell, C, F., Schmidt, D, P., 2016, JSAE Review.
[11] Guo, H., Ding, H., Li, Y., Ma, X., Wang, Z., Xu, H., 2017, Fuel, 199, pp. 125–34.
[12] Wood, A., Wigley, G., Helie, J., July 07.-10. 2014, 17th International Symposium on Applications of Laser Techniques to Fluid Mechanics.
[13] Lacey, J., Poursadegh, F., Brear, M. J., Gordon, R., Petersen, P., Lakey, C., 2017, Fuel, 200, pp. 345–56.
[14] Moulai, M., Grover, R., Parrish, S., Schmidt, D., 2015, SAE Technical Paper, 01, 0944.
[15] Allocca, L., Montanaro, A., Gioia, R. Di., Bonandrini, G., 2014, SAE Technical Paper, 32, 0041.
[16] Montanaro, A., Allocca, L., 2015, SAE Technical Paper, 01, 1945
[17] Serras-Pereira, J., Van, Romunde, Z., Aleiferis, P. G., Richardson, D., Wallace, S., Cracknell, R. F., 2010, Fuel, 89, pp. 2592–607
[18] Price, C. J., Hamzehloo, A., Aleiferis, P., Richardson, D., 2015, SAE Technical Paper, 24, 2463.
[19] Oza, R., Sinnamon, J. F., 1983, SAE Technical Paper, 830590.
[20] Engine Combustion Network, https://ecn.sandia.gov
[21] Drew, A. D., and Passman, S. L., 1999, “Theory of Multicomponent Fluids.”
[22] Edwards, A. R., and O’Brien, T. P., 1970, Journal of Br. Nuclear Energy, 9, pp. 125-135
[23] CSNI International Standard Problems (ISP), Report NEA/CSNI/R(2000)5.